Bulletin of the Seismological Society of America, Vol. 96, No. 3, pp. 957–967, June 2006, doi: 10.1785/0120050061

Characterization of the Sedimentary Cover of the Zafarraya Basin, Southern Spain, by Means of Ambient Noise

by Antonio García-Jerez, Francisco Luzón, Manuel Navarro, and J. Alfonso Pérez-Ruiz

Abstract The sedimentary structure in the Zafarraya basin, located in the south of Spain, is studied by using the horizontal-to-vertical spectral ratio (HVSR) for ambient noise. To improve the reliability of the results, the stability of the HVSR measurement was checked by using a time-dependent analysis of the noise records taking into account only clear peaks. The resonant frequency varies through the basin and does not ever coincide with the maximum of the horizontal power spectrum.

Several fits between the frequency of the main peak in the HVSR for microtremors and the depth to the bedrock are obtained for data from 17 sites, where geotechnical information was available. The relation derived using a scheme based on surface waves was considered to be the most reliable one. Thus, a function describing the average velocity versus depth for the sedimentary cover of the basin is also derived under assumptions of lateral homogeneity and smooth vertical variations of velocity due to age and/or confining pressure.

The measurement of microtremors at 86 uniformly distributed points provides a map of the sedimentary thickness based on the previously calculated relationships, showing values greater than 200 m at the deeper zones.

Introduction

Site effects are very important in the evaluation of seismic hazard. Since the earlier work of Kanai (1954), many efforts have been devoted to obtaining relevant soil characteristics based on cheap and rapid methods like the analysis of ambient noise (microtremors). The origin of this kind of vibration is due to human activities and atmospheric phenomena (Taga, 1993; Bard, 1999). Extracting geological information from noise records is not an easy task and several schemes are currently being used in a complementary way. The most powerful methods are based in the analysis of simultaneous records of the wave field, either dealing directly with space correlations of temporal records (Aki, 1957) or using the frequency-wavenumber representation (Capon, 1969). Many studies (Nakamura, 1989; Lermo and Chávez-García, 1994) have shown that some information may indeed be obtained even from a single-station noise record using the ratio of the horizontal Fourier spectra to the vertical spectrum (HVSR). When a homogeneous soft sedimentary cover exists and has a high enough mechanical contrast with the underlying materials the resonant frequency appears in the HVSR corresponding approximately at the value $f = \beta/4h$ where β is the shear velocity in the soft layer and h is its thickness.

The aim of this article is to obtain a better knowledge of the structure of the Zafarraya basin (Fig. 1), a large karstic depression located in the south of the Iberian Peninsula (López-Chicano *et al.*, 2002), by using the horizontal-to-vertical spectral ratio (HVSR) jointly with a slight generalization of the soil model, which takes into account the possibility of smooth variations of the shear velocity through the sedimentary layer (Ibs-von Seht and Wohlenberg, 1999).

The studied basin is located in a region that suffers the highest seismic hazard in the Iberian Peninsula because of the collision between the Euroasiatic and the African plates. An example of that was the Andalusian earthquake, with magnitude 6.8 according to the Instituto Andaluz de Geofisica (www.ugr.es/~iag) and epicentral intensity X, which caused heavy damage on the 24 December 1884. Few works have been published about the seismic response of the Zafarraya basin. The earlier studies using records of ambient noise were presented by Morales (1991) and Morales *et al.* (1991), who performed an analysis of the horizontal motion at 15 locations along two perpendicular profiles (approximately from the point I1 to L4 and from E5 to K2 in Fig. 1). They found a dominant frequency at about 3 Hz, which remained almost constant within the entire surface of the basin. These results were confirmed by numerical computations using 2D models (Schenková and Zahradnik, 1996). Luzón (1995) and Luzón *et al.* (2004) carried out numerical simulations for 2D and 3D homogeneous models of this basin under the incidence of plane waves using the indirect boundary element method (IBEM). They found amplifications of

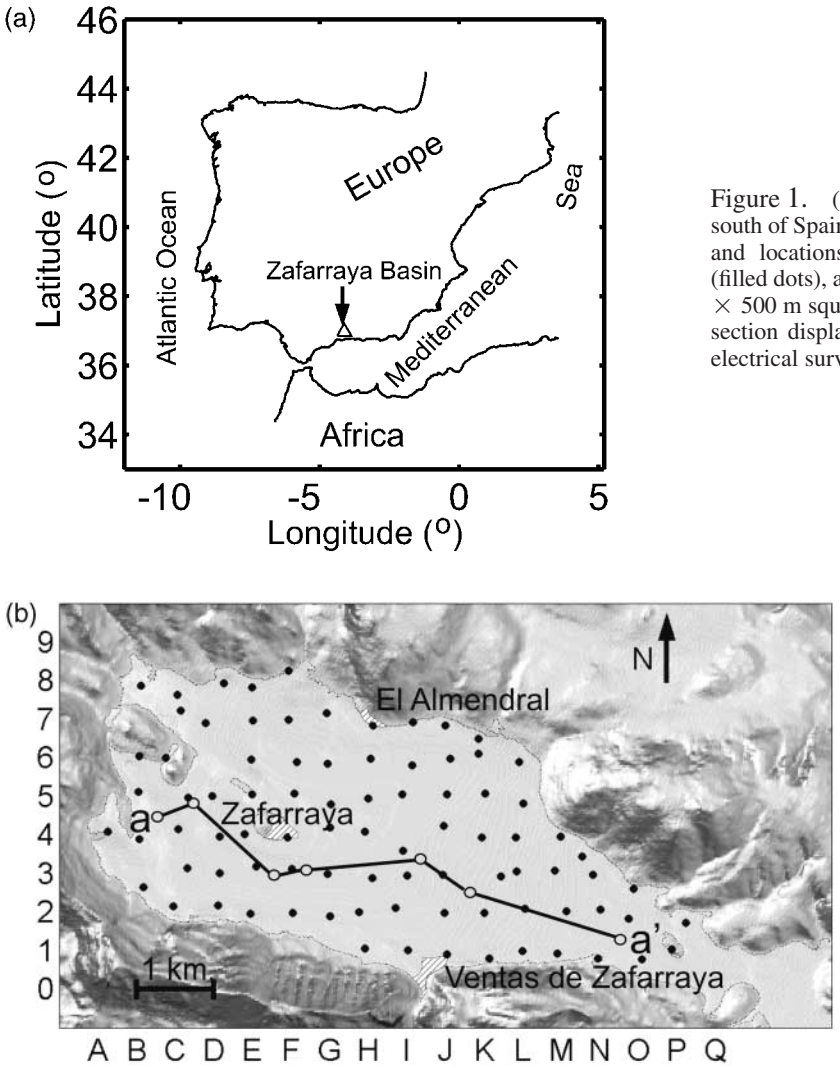

Figure 1. (a) Location of the Zafarraya basin in the south of Spain. (b) Topography of the Zafarraya basin and locations where ambient noise was recorded (filled dots), approximately on the vertices of a 500 m × 500 m square grid. The black line shows the cross section displayed in Figure 2, joining a set of geoelectrical surveys (open dots).

ground motion up to 12 times the amplitude of the incoming wave over the deeper zones and showed that the fundamental resonant frequency depended on the local depth of the basement.

Geological Settings

The Zafarraya basin is a large (22 km^2) Neogene karstic hollow located in southwest Spain and enclosed in the Betic Mountains. It has a length of about 10 km following a general east-southeast–west-northwest trend (Fig. 1). The maximum width (3.5 km) appears in its occidental sector. The altitude is about 900 m over the sea level, decreasing slowly toward the east and north directions. The north part is limited by a big carbonated mass of Jurassic white limestone called "Sierra Gorda," whereas the other edges are occupied by the Zafarraya mountains composed of dolomitic limestone.

Several researches have been performed in this area using geoelectrical (López-Chicano, 1989) and geotechnical surveys (Martín Vivaldi *et al.*, 1971), revealing a certain complexity in the sedimentary structure of the basin. These studies show a shallower layer composed by sand, silt, and alluvial conglomerates that goes from the surface to less than 10 m at its deeper point (López-Chicano, 1992). A geological sketch for a longitudinal section is shown in Figure 2. Clay and alluvial silt constitute a second layer with a maximum thickness of about 50 m in the oriental sector. These materials lie directly on the stiff Mesozoic carbonated basement in the west. Next to the southern edge and in the central part there is a thick layer of marls, which are replaced by calcarenites mainly in the east. The depth of this stratum down to the older limestone is not well determined, although it is known that it reaches 200 m at least in some zones around the bed of the Madre River (López-Chicano, 1992). This seasonal stream flows from the southeast to the swallow holes at the northwest edge, losing 60% of water before reaching the center of the basin because of the large infiltration through the alluvial deposits. Minor streams and swallows are located mainly in the western border, which is a complicated area because of the outcropping of the under-

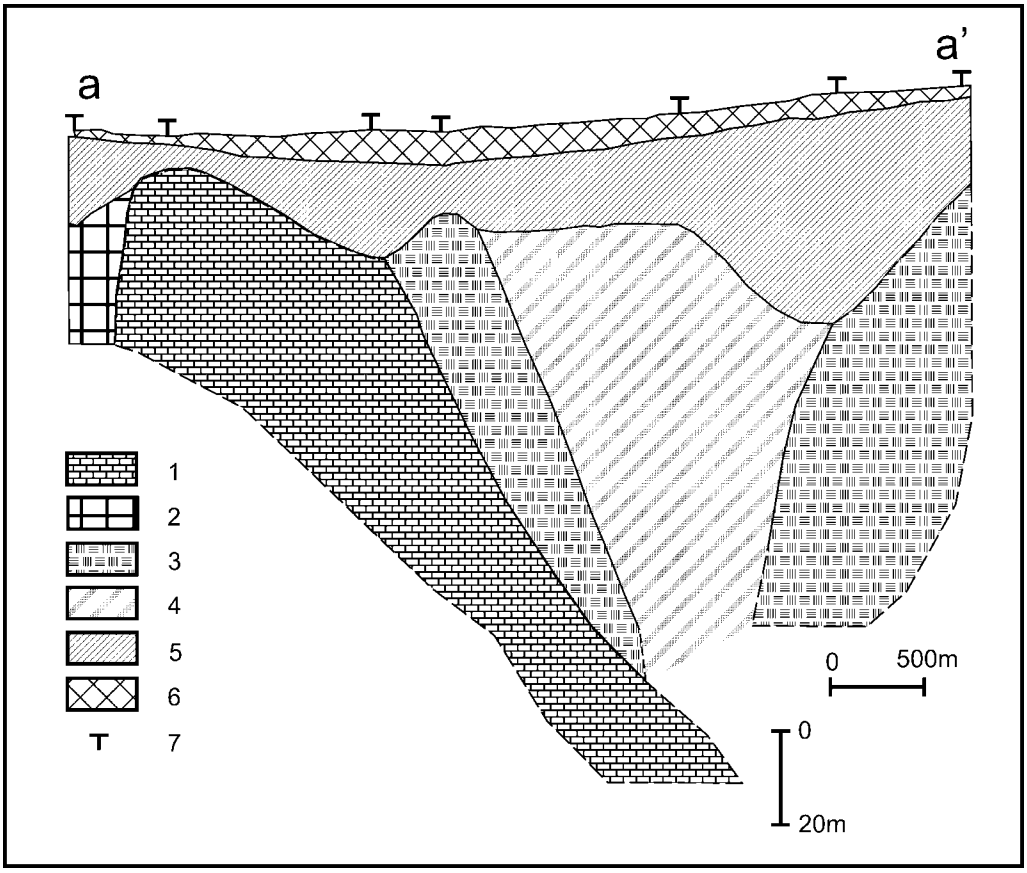

Figure 2. Geological cross section of the Zafarraya basin along the black line shown in Figure 1. 1, Mesozoic carbonated materials; 2, marly and calcareous materials of the cretaceous period; 3, calcarenites; 4, bluish marls of the upper Miocene epoch; 5, clay and alluvial silt; 6, sand, silt, and alluvial conglomerates; 7, geoelectrical survey. Adapted from López-Chicano (1992).

lying limestone. More information about the hydrogeology of this zone may be found in López-Chicano *et al.* (2002).

Several small villages are placed at the edges of the basin, such as Zafarraya at the western outcroppings or Ventas de Zafarraya at the central part of the southern border (see Fig. 1), whereas most of the surface of the basin is used for agricultural cultivation.

Microtremor Measurement

In July 2004, 86 microtremor records were obtained approximately on the vertices of a regular grid composed of 500 × 500 m cells covering the Zafarraya basin (Fig. 1). In contrast to Morales *et al.* (1991), who used only horizontal components, we recorded the three components of ambient noise. The instruments used were two short-period three-component seismographs working with a sampling frequency of 100 Hz. One of them consists of an SPC-35 digitizer and three VSE-15D sensors with measuring frequency range between 0.25 and 70 Hz. The other one uses Mark L4-C sensors that provide an acceptable response in the range between 0.65 and 40 Hz. Both devices have been employed in several previous works (Navarro *et al.*, 2001; Almendros *et al.*, 2004; Al Yuncha *et al.*, 2004). The sensors were fixed on leveled platforms placed directly on the ground. The operations of farm machinery that produced continuous noise were stopped around each measured point.

The recording time was 10 min and the details of the signal processing followed Almendros *et al.* (2004), based in the use of ratiograms. After instrumental corrections, each record was divided in a set of overlapping windows of 20.48 sec centered each 2.56 sec. This length is suitable for the numerical fast Fourier transform (FFT) algorithm and contains 10 periods, at least, for any frequency larger than 0.5 Hz. Frequency-dependent window lengths have also been used in the literature keeping constant the number of cycles (see, for example, Kind *et al.*, 2005). The spectral ratio is computed separately for all time intervals and plotted in a time-dependent diagram (ratiogram) as shown in Figure 3b. Then, the velocity record is visually inspected and the HVSRs are averaged over the good-quality zones, avoiding transients due to close sources like cars or footsteps. Other choices of the window lengths (30 sec and 40.96 sec) and

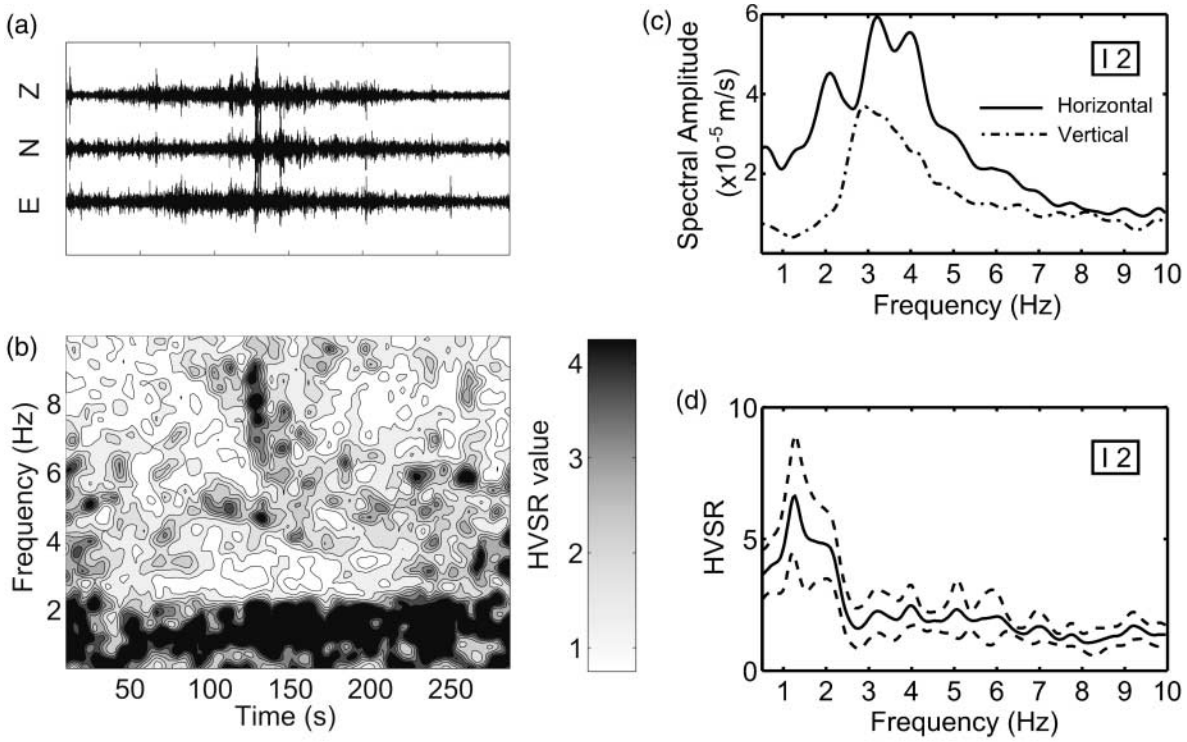

Figure 3. Stability analysis of HVSR for point I2. (a) Three component records of noise. (b) Time-dependent spectral ratio. (c) Time-averaged horizontal (solid line) and vertical (dash-dot line) spectral amplitudes. (d) Average spectral ratio (solid line) and average plus or minus one standard deviation (dashed lines). Notice the discrepancy between the frequency of maximum amplitude in the horizontal spectrum and the frequency of resonance (defined as the position of the main peak in the HVSR).

lower overlapping ratios (10%) have been tested without significant variations in the results.

This method allowed us to find resonant frequencies at different locations in a wide spectral range in contrast to the results of Morales *et al.* (1991). The stability of the main peak was checked and unclear results were not considered, that is, those results in which the observed peaks were not stable during all the time of the ratiogram. Although a high spectral level was sometimes found at about 3 Hz in the horizontal component, it does not always match the main peak in the HVSR, as shown in Figure 3c and d. Some examples of the spectra of the components and the resulting ratios for three places are displayed in Figure 4. The peak frequencies for points where a dominant resonance was clearly identified are shown in Figure 5.

Fit of Shear-Velocity Profile and Frequency-Depth Relationship

Inside any sedimentary layer composed of approximately homogeneous geological materials, the shear module increases smoothly with depth (but much faster than the density) because of the confining pressure. This variation of the shear velocity may be expressed as the function (see, for example, Ibs-von Seht and Wohlenberg, 1999):

$$\beta(z) = \beta_0\left(1 + \frac{z}{z^*}\right)^x, \quad z < h, \tag{1}$$

where β is the shear velocity at a given depth z in the sedimentary layer ($0 < z < h$), β_0 is the velocity at the ground surface, x is a parameter giving the depth dependence, and z^* is a reference distance that controls the behavior for small values of z. The fundamental resonant frequency for such a sedimentary structure may be estimated, considering vertical *S*-wave incidence, from the travel time in the layer (Ibs-von Seht and Wohlenberg, 1999):

$$\frac{1}{4f} = \int_0^h \frac{dz}{\beta(z)}. \tag{2}$$

From (1) and (2) we obtain:

$$h(f) = z^*\left[\beta_0\frac{(1 - x)}{4fz^*} + 1\right]^{1/(1-x)} - z^*. \tag{3}$$

Equation (3) gives the thickness h of the sedimentary cover from the empirical measurement of the resonant frequency f and a previous fit of the free parameters x, β_0, and z^*. A

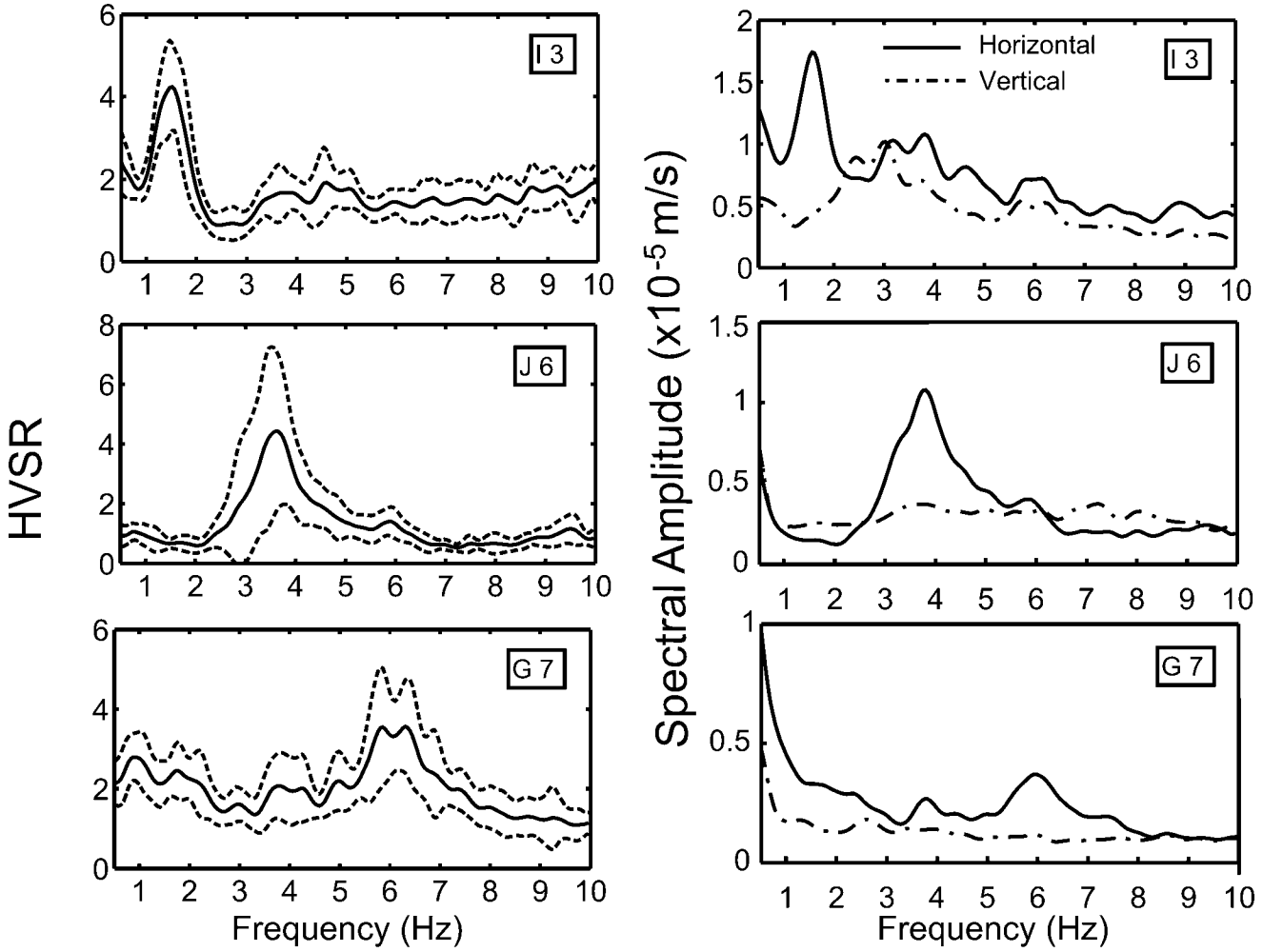

Figure 4. Examples of HVSRs (solid lines) and spectral amplitudes for several points (I3, J6, and G7) with decreasing sediment thickness. The type of lines has the same meaning as in Figure 3(c) and (d).

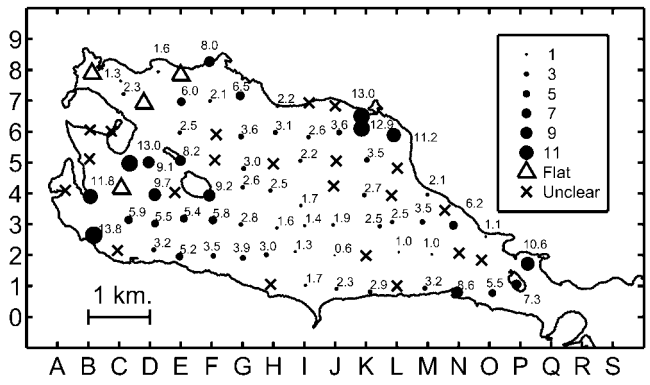

Figure 5. Map of resonant frequencies in hertz obtained from HVSR. Sites where the ratio shows several similar peaks or an unclear (low stability) peak are marked by an X. A triangle marks points with nearly flat ratios or high-frequency broad peaks (15 Hz or larger).

slightly simpler approach is used in Delgado *et al.* (2000a,b) which corresponds to a power depth–velocity law:

$$\beta'(z) = \beta_0\left(\frac{z}{z^*}\right)^x. \tag{4}$$

$\beta'(z)$ is a good approximation of $\beta(z)$ for $z \gg z^*$. In that case, with $x < 1$, equation (2) leads to:

$$h'(f) = \left(\frac{(1 - x)\beta_0}{4fz^{*x}}\right)^{1/(1-x)}. \tag{5}$$

This equation could lead to a linear fit in logarithmic scale with a value of the slope $B = 1/(1 - x)$.

To carry out the adjustment of the free parameters for the Zafarraya basin, a set of 17 grid locations was considered where the depth of the sedimentary layer is well determined by means of close geoelectrical surveys and where the resonant frequency was clearly measured. The selected points

give the dashed line shown in Figure 6a using a nonlinear least-squares fit for equation (3). The fitted values of z^* were much lower than the depth of the shallower considered point (11 m), thus z^* may be fixed to 1 m for simplicity without influence in the range of data.

The resulting equation, for depths from 11 to 125 m, is

$$\beta(z) = 437(1 + z)^{0.136}, \tag{6}$$

where β is in meters per second and z is in meters. The root-mean-square error of the data is about 6 m with regard to the function in equation (6) (see Table 1). It may be considered a rough estimate of the depth errors. The ranges for the parameters considering 68% and 95% confidence levels (see Nash and Sofer, 1996; Press *et al.*, 1992, among others) are also given in Figure 6b. Uncertainties in depth data (standard deviations of h for each survey) are poorly known and have not been considered in the fit. A minimization of the sum of squared differences between experimental and calculated depths has been chosen for obtaining equation (6). This criterion is equivalent to assuming that the variances in f are negligible, and the variances in h take a unique value for all grid locations (see, for example, Press *et al.*, 1992). Note that the kind of fit may significantly influence the final relationship, that is, the result is influenced by the choice of the independent variable when standard deviations of the data are not included in the misfit estimator. For example, the deviations between experimental and calculated depths are not equally weighted if the fit is performed in terms of $\log(h)$ (as in Delgado *et al.*, 2000b). In this case the parameters $\beta_0 = 375$ m/sec and $x = 0.185$ for the Zafarraya soil model are those which minimize the sum of the misfits in $\log(h)$.

Taking into account that seismic noise seems to be composed mainly of surface waves (Konno and Ohmachi, 1998), an alternative approach can be followed by using the scheme described in Arai and Tokimatsu (2000) for the forward computation of the resonant frequency instead of equation (2). In this scheme, the horizontal ($P_H(\omega)$) and vertical ($P_V(\omega)$) power spectra on the free surface, due to a distribution of infinite impulsive surface point sources located at random positions over a 1D structure, is computed by means of a summation (m index) of Rayleigh and Love wave normal modes. Let us assume that $L_V(\omega)$ is the vertical component of the point forces and $L_H(\omega)$ is the horizontal component (arbitrarily directed), then, the following equations are obtained:

$$P_V \cong \xi \sum_m \left(\frac{A_{Rm}}{k_{Rm}}\right)^2 \left[1 + \left(\frac{\alpha^2}{2}\right)\left(\frac{\dot{u}}{\dot{w}}\right)_m^2\right] \tag{7}$$

$$P_H \cong \xi \sum_m \left(\frac{A_{Rm}}{k_{Rm}}\right)^2 \left(\frac{\dot{u}}{\dot{w}}\right)_m^2 \left[1 + \left(\frac{\alpha^2}{2}\right)\left(\frac{\dot{u}}{\dot{w}}\right)_m^2\right] + \xi \sum_m \left(\frac{\alpha^2}{2}\right)\left(\frac{A_{Lm}}{k_{Lm}}\right)^2, \tag{8}$$

where $(\dot{u}/\dot{w})_m$ is the ellipticity of the m Rayleigh mode, defined in Haskell (1953); $A_{Rm}(\omega)$ and $A_{Lm}(\omega)$ are the medium response factors for Rayleigh and Love waves defined in Harkrider (1964); k_R and k_L are the respective wavenumbers,

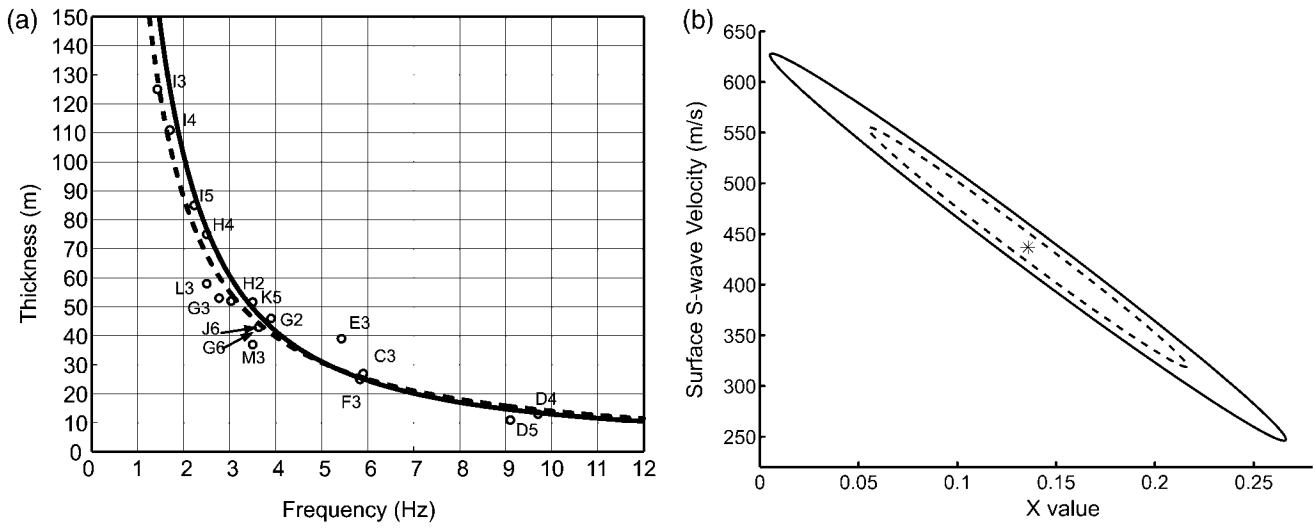

Figure 6. (a) Frequencies of the main peak of HVSR versus depth of the resistive basement computed from geoelectrical surveys. The dashed black line shows the relationship (6) obtained for the Zafarraya basin. The solid black line shows the alternative relationship based on surface waves (equation 10). (b) Error ellipses for the fitted parameters x and β_0 of equation (6) considering 68.3% (dashed line) and 95% (solid line) confidence levels.

Table 1
Statistics of Fit between the Frequency of Resonance (f) and the Thickness of the Sedimentary Cover (h) for Equation (6)

Parameter	Value	Standard Error	Root-Mean-Square Error (m)
β_0 (m/sec)	437	78	6.2554
X	0.1357	0.0534	

$\alpha = L_H/L_V$ and ξ is a common constant for both expressions. The parameter α determines the relative weight of Love waves and Rayleigh waves. (The power of Love waves increases as α rises; thus, only Rayleigh waves are considered for $\alpha = 0$.) Thus, the theoretical spectral ratio is computed as:

$$\text{HVSR} = \sqrt{\frac{P_H}{P_V}}. \tag{9}$$

This method has been recently used for *S*-wave velocity profiling from the HVSR shape (Arai and Tokimatsu, 2004; Parolai *et al.*, 2005).

The theoretical resonant frequency was taken from the simulated HVSR for the sites where the depth was known and for each couple of parameters (β_0, x). For these calculations, the sediments were divided into as many 5-m-thick layers as necessary with *S*-wave velocity obtained from equation (1), taking a suitable value of 2000 m/sec for the carbonated bedrock (Schenková and Zahradnik, 1996). The horizontal-to-vertical load ratio α was taken as the unity and every mode of surface wave acting within a wide enough range around the first peak (resonant frequency) was considered in the calculation. The densities were taken as 2.1 g/cm^3 for the sedimentary cover and 2.5 g/cm^3 for the bedrock and 0.25 was used for the Poisson's ratio. The best fit between computed and measured frequencies was:

$$\beta(z) = 214(1 + z)^{0.305}, \tag{10}$$

which corresponds to the solid line in Figure 6a. The root mean error for this fit is 0.64 Hz. Some examples of HVSRs computed considering surface waves for several values of α are shown by solid black lines in Figure 7 for point K5 (with 52 m of basement depth) using the soil model defined by (10). The HVSRs simulated for surface waves show a good agreement with the main observed frequency of the measurement (solid gray line), although these simulations do not give the amplitude of the peak. Anyway, the amplitude level is not relevant in this fit, but to the fitted frequency.

Note that the assumptions about the way to compute resonant frequencies have a significant influence on the soil model inferred. The result based on surface waves (equation 10) is considered to be a better approximation to the real properties than equation (6), because equation (2) is not an exact estimation of the resonant frequency for vertically incident *S* wave in heterogeneous media (see the significant difference between the first maximum of the transfer function shown by a dashed black line in Fig. 7 and the resonant frequency computed from the travel time shown by a vertical dashed line). The use of a method based on surface waves (including Love waves) has been preferred because microtremor is mainly composed of this kind of waves. This fact is supported by many previous works that deal with this topic using experimental and/or theoretical approaches (see, for example, Aki, 1957; Lachet and Bard, 1994; Tamura, 1996; Konno and Ohmachi, 1998; Arai and Tokimatsu, 2000; Ohori *et al.*, 2002).

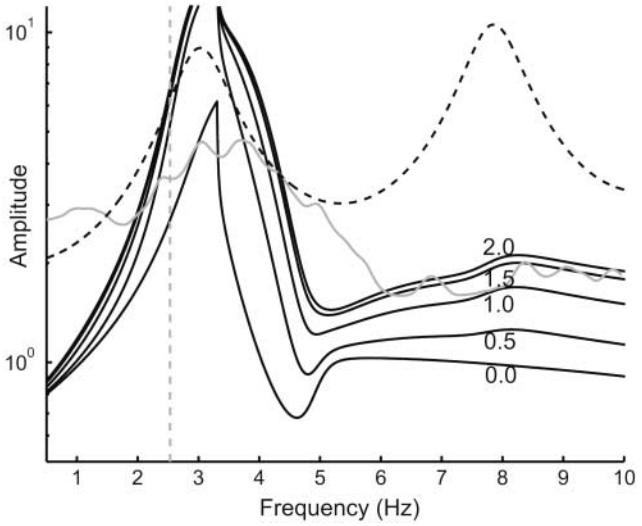

Figure 7. Measured (solid gray line) and theoretical (solid black lines) HVSRs for point K5 by using the soil model of equation (10) down to the bedrock. Labels indicate the corresponding value of the load ratio α. Dashed black line shows the 1D transfer function for vertically incident *S* waves. Vertical dashed line shows the resonant frequency computed for the structure from equation (2).

Discussion

The *f-h* relationships obtained for the sedimentary cover of the Zafarraya basin are compared in Figure 8 with those found in previous works, which are listed, among others, in Table 2 (Parolai *et al.*, 2002, for the Cologne Area; Delgado *et al.*, 2000a, for the Segura river valley; and Ibs-von Seht and Wohlenberg, 1999, for the Lower Rhine Embayment). In those studies where a strict f versus h power law was derived ($h = Af^B$) it is possible to obtain β_0 and x from equation (5), taking $z^* = 1$ m. The functions $\beta(z)$ derived from these areas are represented in Figure 9 together with the models for the Zafarraya basin of equations (6) and (10).

The parameters β_0 and x depend on the geological characteristics of the basin. Nevertheless, the exponents show smaller relative variations (Table 2), especially if the comparison is performed in terms of $B = 1/(1 - x)$ (exponent

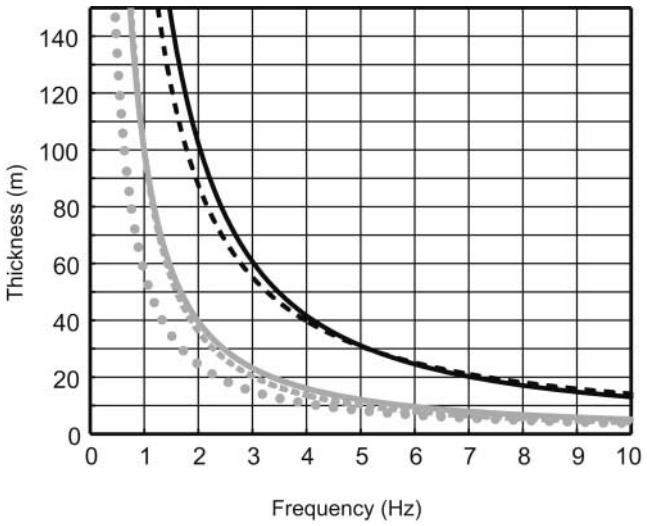

Figure 8. Comparison of f versus h relationships for the Zafarraya basin derived from equation (2) (dashed black line) and from a scheme based on surface waves (solid black line). The results of similar studies performed in other places are also displayed. The result for the lower Rhine embayment (Ibs-von Seht and Wohlenberg, 1999) is drawn with a solid gray line, that for the Cologne area (Parolai *et al.*, 2002) is shown with a dashed line, and the formula for the Segura river valley (Delgado *et al.*, 2000a) is shown with a dotted gray line.

of the *f–h* relationship), as was noticed by Delgado *et al.* (2000a). Both parameters have also been studied in the literature with other methodologies. For example, Ohta and Goto (1978) obtained an empirical power relationship between β and z from geotechnical data with an exponent $x = 0.312$ ($B = 1.454$) and β_0 depending on the soil textural class. More detailed expressions (Hardin and Drnevich, 1972) show that the shear modulus G in particulate soils is approximately proportional to the square root of the effective stress σ_0 and also depends on some geotechnical parameters (mass density of the particles, saturation degree, void ratio, plasticity index, and overconsolidation ratio). Thus, β is proportional to $z^{0.25}$ only when these geotechnical parameters remain constant within the sedimentary layer (see, for example, Schneider *et al.*, 1999). Previous works listed in Table 2 show values larger than 0.25 except for the Segura river valley ($x = 0.204$ or $B = 1.256$) where very shallow sediments (down to 45.7 m) and softer soils were mostly considered. Larger values of x as 0.28 and 0.37 ($B = 1.388$ and 1.587, respectively) have been found for the places with thicker sedimentary cover containing cemented materials and soft sedimentary rocks that are characterized by a higher stiffness (see, for example, Kramer, 1996). Moreover, exponents of 0.448 ($B = 1.812$) have been obtained for the bedrock in the Cologne area between 20 and 377 m (Parolai *et al.*, 2002). The comparison of the values obtained here with other sedimentary deposits give us confidence to assess that 0.305 (from equation 10, obtained considering that microtremors are composed of surface waves) is a reliable value for the x parameter at the Zafarraya basin.

Table 2
Exponent of the z Versus β Relationship (x) and Surface Velocity (β_0) for Several Sedimentary Structures

Location	x	β_0 (m/sec)
Zafarraya Basin (based on equation 1)	0.136	437
Zafarraya Basin (surface-wave scheme)	0.305	214
Lower Rhine Embayment (Budny, 1984)	0.278	162
Lower Rhine Embayment (Ibs-von Seht and Wohlenberg, 1999)	0.280	148.8
Cologne Area (Parolai *et al.*, 2002)	0.37	115
Segura River Valley (Delgado *et al.*, 2000a)	0.204	122.3

The z^* parameter which controls the shape of the function close to the surface has been fixed in 1 m.

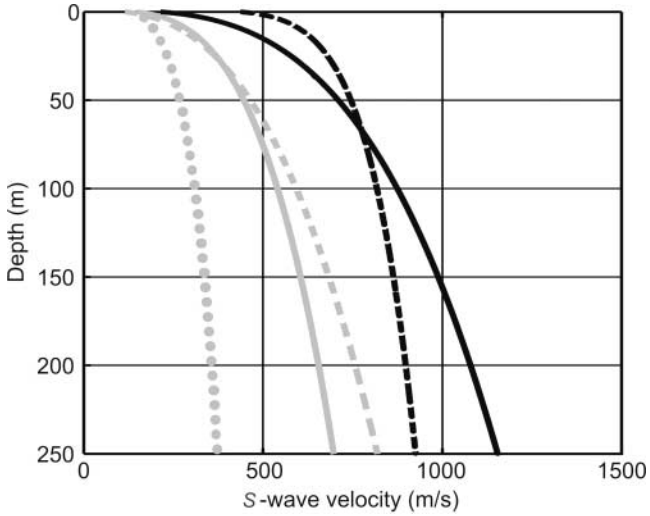

Figure 9. Shear velocity versus depth for sedimentary materials up to the stiff bedrock. The lines are computed from the studies shown in Figure 8 and using the same type of lines and symbols.

The main result of this work is the improved map of the basement shown in Figure 10, which results from the interpolation of the depths computed using equation (10) for points where the dominant period could be determined. The most important feature is the increasing depth in the direction to the central part, near the southern edge (see Fig. 11 for cross sections along columns C, F, I, and L). This trough in the underlying carbonated rock spreads toward the east throughout the bed of the stream. The thickness of the sedimentary cover decreases faster to the south and west than to the north and east. For the southwestern sector, next to the southern edge of the basin (points D2, E2, and F2), we found values lower than 50 m that seem to be underestimated in comparison with Morales *et al.* (1991) or López-Chicano (1992) who gave depths reaching 90 m and greater than 100 m, respectively, up to a highly resistive basement. HVSRs show low amplitudes (around 2) for the main peak

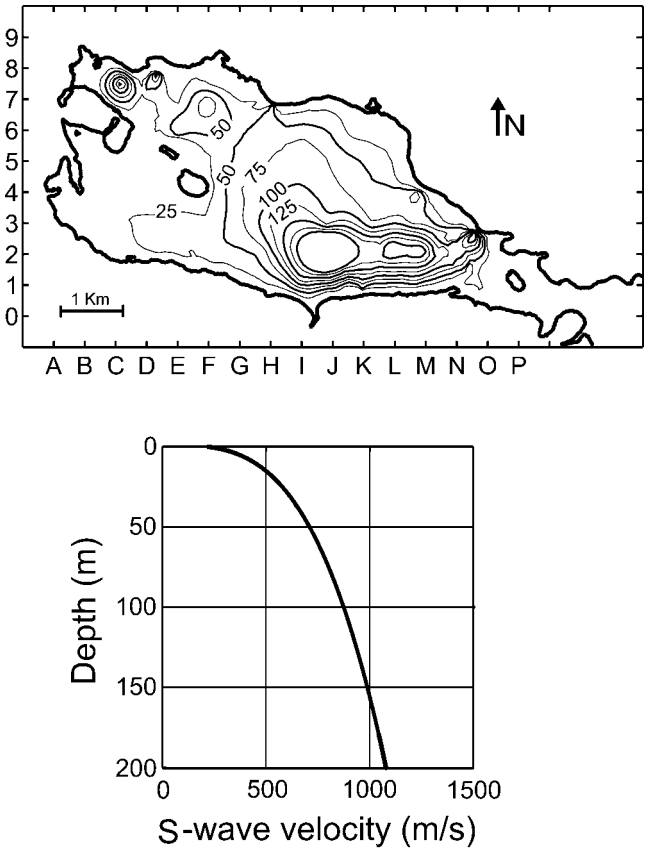

Figure 10. Thickness of the sedimentary cover interpolated for the studied area. The *S*-wave velocity of the model depends only on the depth and is given for the sediments by equation (10) shown, which has been extrapolated down to 200 m.

at that zone of the basin, suggesting a poor impedance contrast between the sediments and the bedrock. The presence of sedimentary materials with anomalous (larger) *S*-wave velocity should be the explanation of such underestimated depth. The spectral ratio has also been computed separately by using the north–south and the (east–west horizontal components near the southern edge to check possible 2D effects, but no differences were found between both magnitudes. The existence of an increase of the sediment thickness at the northwestern area, just north of the rock outcrops (point E6) and at the northern edge close to the main swallow (C7, C8, and D8) agrees with the results of López-Chicano (1992), although it is not coherent with the depth shown by Morales *et al.* (1991).

Concluding Remarks

The depth of the sedimentary materials that fill the Zafarraya basin has been studied by using the HVSR for ambient noise. We obtained a variation of the frequency of resonance, in contrast with previous works (Morales, 1991; Morales *et al.*, 1991; Schenková and Zahradnik, 1996), which pointed to a common peak at about 3 Hz independent of local depth. Note that the analysis of spectral ratios sometimes leads to different results compared with the analysis of the horizontal component of microtremors as performed by Morales (1991). An example of that is shown in Figure 3c and d corresponding to the point I2.

A dataset from geoelectrical surveys let us fit relations between the predominant frequency for each place and its corresponding thickness of soft soil. *S*-wave velocity–depth-averaged functions (equations 6 and 10), valid for each point down to the level of the basement, are derived under the hypothesis of lateral homogeneity in the geological characteristics of the sediments.

From the measurement of microtremors in a dense grid, a map of bed topography has been developed showing a good agreement with previous works and with the qualitative geological information. This contributes new results about poorly studied zones like the eastern edge of the basin. Our results will allow us to improve our knowledge about the dynamic behavior of the basin to perform an accurate evaluation of its seismic hazard.

Acknowledgments

This research was supported by CICYT grants REN2002-04198-C02-02/RIES, CGL2005-05500-C02-02/BTE, and REN2003-08159-C02-01, by the European Community with FEDER, and the research team RNM-194 of Junta de Andalucía (Spain). We gratefully acknowledge the generous cooperation of A. Posadas, C. F. Aguilera, and S. Limonchi in the observations of seismic noise. We are very grateful to two anonymous referees for their constructive reviews, which significantly improved this article.

References

Aki, K. (1957). Space and time spectra of stationary stochastic waves, with special reference to microtremors, *Bull. Earthquake Res. Inst.* **35,** 415–456.

Almendros, J., F. Luzón, and A. Posadas (2004). Microtremors analysis at Teide Volcano (Canary Islands, Spain): assessment of natural frequencies of vibration using time-dependent horizontal-to-vertical spectral ratios, *Pure Appl. Geophys.* **161,** 1579–1596.

Al Yuncha, Z., F. Luzón, A. Posadas, J. Martín, G. Alguacil, J. Almendros, and S. Sánchez (2004). The use of ambient seismic noise measurements for estimation of surface soil effects: the Motril City case (Southern Spain), *Pure Appl. Geophys.* **161,** 1549–1559.

Arai, H., and K. Tokimatsu (2000). Effects of Rayleigh and Love waves on microtremor H/V spectra, Presented at *Proc. 12th World Conf. on Earthquake Engineering*, paper 2232.

Arai, H., and K. Tokimatsu (2004). *S*-wave velocity profiling by inversion of microtremor H/V spectrum, *Bull. Seism. Soc. Am.* **94,** 53–63.

Bard, P. Y. (1999). Microtremor measurements: a tool for site effect estimation?, *The Effects of Surface Geology on Seismic Motion*, Vol. 3, Balkema, Rotterdam, 1251–1279.

Budny, M. (1984). Seismische Bestimmung der bodendynamischen Kennwerte von oberfläschennahen Schichten in Erdbebengebieten der Niederrheinnischen Bucht und ihre ingenieurseismologische Anwendung, *Geol. Inst. Univ. Cologne* special issue 57.

Capon, J. (1969). High-resolution frequency-wavenumber spectrum analysis, *Proc. IEEE* **57,** no. 8, 1408–1418.

Delgado, J., C. López Casado, A. C. Estévez, J. Giner, A. Cuenca, and S.

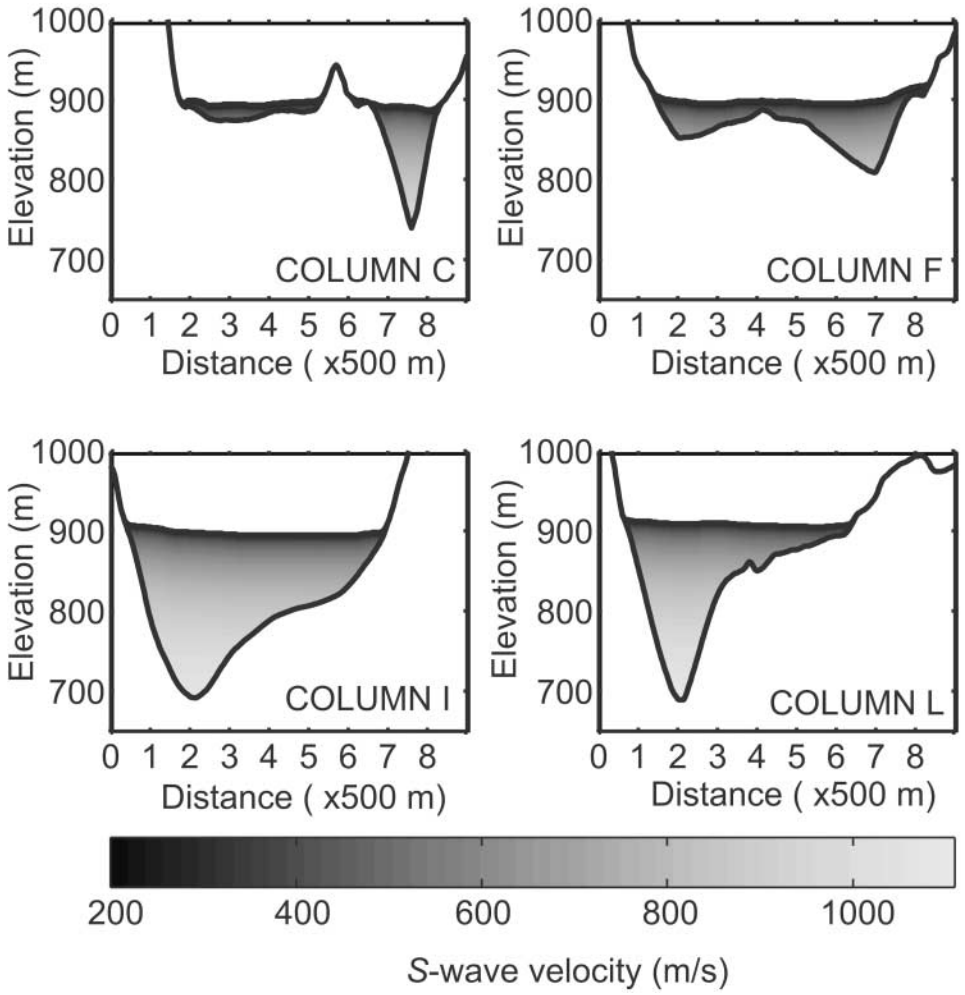

Figure 11. Cross sections of the Zafarraya basin through columns C, F, I, and L of Figure 10, showing the relief and the estimated depth of sediments down to the limestone. A gray scale indicates the *S*-wave velocity.

Molina (2000a). Mapping soft soils in the Segura river valley (SE Spain): a case study of microtremors as an exploration tool, *J. Appl. Geophys.* **45,** 19–32.

Delgado, J., C. López Casado, J. Giner, A. C. Estévez, A. Cuenca, and S. Molina (2000b). Microtremors as a geophysical exploration tool: applications and limitations, *Pure Appl. Geophys.* **157,** 1445–1462.

Hardin, B. O., and V. P. Drnevich (1972). Shear modulus and damping in soils: design equations and curves, *J. Soil Mech. Found. Div. Am. Soc. Civ. Eng.* **98,** 667–692.

Harkrider, D. G. (1964). Surface waves in multilayered elastic media. Part 1, *Bull. Seism. Soc. Am.* **54,** 627–679.

Haskell, N. A. (1953). The dispersion of surface waves on multilayered media, *Bull. Seism. Soc. Am.* **43,** 17–34.

Ibs-von Seht, M., and J. Wohlenberg (1999). Microtremor measurements used to map thickness of soft sediments, *Bull. Seism. Soc. Am.* **89,** 250–259.

Kanai, K., T. Tanaka, and K. Okada (1954). Measurement of the microtremor. I, *Bull. Earthquake Res. Inst.* **32,** 199–210.

Kind, F., D. Fäh, and D. Giardini (2005). Array measurements of S-wave velocities from ambient vibrations, *Geophys. J. Int.* **160,** 114–126.

Konno, K., and T. Ohmachi (1998). Ground-motion characteristics estimated from spectral ratio between horizontal and vertical components of microtremor, *Bull. Seism. Soc. Am.* **88,** 228–241.

Kramer, S. L. (1996). *Geotechnical Earthquake Engineering*, Prentice Hall, Upper Saddle River, New Jersey.

Lachet, C., and P. Y. Bard (1994). Numerical and theoretical investigations on the possibilities and limitations of Nakamura's technique, *J. Phys. Earth* **42,** 377–397.

Lermo, J., and F. J. Chávez-García (1994). Are microtremors useful in the site response evaluation? *Bull. Seism. Soc. Am.* **84,** 1350–1364.

López-Chicano, M. (1989). Geometría y estructura de un acuífero kárstico perimediterráneo: Sierra Gorda (Granada y Málaga), *Master's Thesis*, University of Granada, Spain (in Spanish).

López-Chicano, M. (1992). Contribución al conocimiento del sistema hidrogeológico kárstico de Sierra Gorda y su entorno (Granada y Málaga), *Ph.D. Thesis*, University of Granada, Spain (in Spanish).

López-Chicano, M., M. L. Calvache, W. Martín-Rosales, and J. Gisbert (2002). Conditioning factors in flooding of karstic poljes—the case of the Zafarraya polje (South Spain), *Catena* **49,** 331–352.

Luzón, F. (1995). Determinación de la respuesta sísmica de estructuras geológicas superficiales mediante el método indirecto de elementos en la frontera, *Ph.D. Thesis*, University of Granada, Spain (in Spanish).

Luzón, F., S. A. Gil-Zepeda, F. J. Sánchez-Sesma, and C. Ortiz-Alemán (2004). Three-dimensional simulation of ground motion in the Zafarraya basin (Southern Spain) up to 1.335 Hz under incident plane waves, *Geophys. J. Int.* **156,** 584–594.

Martín Vivaldi, J. L., M. A. Caballero, M. Calle, and R. Lhenaff (1971). Estudio mineralógico de los niveles arcillosos del polje de Zafarraya, Granada (España), *Estudios Geológicos* **27,** 137–144 (in Spanish).

Morales, J. (1991). Caracterización de la respuesta sísmica local de las cuenca de Granada (España) y Ciudad de Guzmán (México) mediante el análisis espectral de microterremotos y terremotos, *Ph.D. Thesis*, University of Granada, Spain (in Spanish).

Morales, J., F. Vidal, J. A. Peña, G. Alguacil, and J. Ibáñez (1991). Microtremor study in the sediment filled basin of Zafarraya, Granada (Southern Spain), *Bull. Seism. Soc. Am.* **81,** 687–693.

Nakamura, Y. (1989). A method for dynamic characteristics estimations of subsurface using microtremors on the ground surface, *Q. Rep. Railway Tech. Res. Inst. Jpn.* **30,** 25–33.

Nash, S. G., and A. Sofer (1996). *Linear and Nonlinear Programming*, McGraw-Hill Companies, New York.

Navarro, M., T. Enomoto, F. J. Sánchez, I. Matsuda, T. Iwatate, A. Posadas, F. Luzón, F. Vidal, and K. Seo (2001). Surface soil effects study using short-period microtremor observations in Almería City, Southern Spain, *Pure Appl. Geophys.* **158,** 2481–2497.

Ohori, M., A. Nobata, and K. Wakamatsu (2002). A comparison of ESAC and FK methods of estimating phase velocity using arbitrarily shaped microtremor arrays, *Bull. Seism. Soc. Am.* **92,** 2323–2332.

Ohta, Y., and N. Goto (1978). Empirical shear wave velocity equations in terms of characteristic soil indexes, *Earthquake Eng. Struct. Dyn.* **6,** 167–187.

Parolai, S., P. Bormann, and C. Milkereit (2002). New relationships between V_s, thickness of sediments, and resonance frequency calculated by the H/V ratio of seismic noise for the Cologne area (Germany), *Bull. Seism. Soc. Am.* **92,** 2521–2527.

Parolai, S., M. Picozzi, S. M. Richwalski, and C. Milkereit (2005). Joint inversion of phase velocity dispersion and H/V ratio curves from seismic noise recordings using a genetic algorithm, considering higher modes, *Geophys. Res. Lett.* **32,** L01303, doi 10.1029/2004GL021115.

Press, W. P., S. A. Teukolsky, W. T. Vetterling, and B. P. Flannery (1992). *Numerical Recipes*, Cambridge University Press, New York, 680–694.

Schenková, Z., and J. Zahradnik (1996). Interpretation of the microtremor spectra at the Zafarraya basin, southern Spain, *Soil Dyn. Earthquake Eng.* **15,** 69–73.

Schneider, J. A., J. L. Hoyos, P. W. Mayne, E. J. Macari, and G. J. Rix (1999). Field and laboratory measurements of dynamic shear modulus of Piedmont residual soils, *Behav. Characteristics Residual Soils Am. Soc. Civ. Eng. Geotechnical Special Publications* **92,** 12–25.

Taga, N. (1993). Earthquake motion and ground conditions, The Architectural Institute of Japan, Tokyo, 315–325.

Tamura, S. (1996). Comparison of body and Rayleigh wave displacements generated by a vertical force on a layered elastic medium, in *Proc. 11th World Conf. on Earthquake Engineering*, paper 1722, CD-ROM.

Departamento de Física Aplicada
Universidad de Almería
Cañada de San Urbano s/n, 04120 Almería, Spain
agj574@alboran.ual.es

Instituto Andaluz de Geofísica
Universidad de Almería
Cañada de San Urbano s/n, 04120 Almería, Spain

Manuscript received 31 March 2005.